Geophys. J. Int. (2006) **165,** 501–515 doi: 10.1111/j.1365-246X.2006.02896.x

Synthesis of scalar-wave envelopes in two-dimensional weakly anisotropic random media by using the Markov approximation

Tatsuhiko Saito

National Research Institute for Advanced Industrial Science and Technology, Central #7, 1-1-1, *Tsukuba, Ibaraki,* 305 - 8567, *Japan.*
E-mail: tatsu-saito@aist.go.jp

Accepted 2005 October 26. Received 2005 October 24; in original form 2004 September 14

SUMMARY

Due to the Earth's inhomogeneity, seismogram envelopes increase in duration and decrease in amplitude with increasing travel distance. Those features have been explained on the basis of the forward scattering in random media using the Markov approximation. Since the conventional studies assumed isotropic random media, they were not realistic enough to represent the anisotropic lithosphere characterized by long horizontal and short vertical correlation distances. Using the Markov approximation, the present study formulates the envelope synthesis in 2-D weakly anisotropic random media characterized by Gaussian and von Kármán-type autocorrelation functions (ACF). Also, wave propagation is numerically simulated with the finite-difference (FD) method; 2 Hz Ricker wavelets propagate through the random media characterized by 4 km s^{-1} average velocity and the Gaussian ACF with 5 km horizontal correlation distance, 2.5 km vertical correlation distance, and 5 per cent rms fractional velocity fluctuation. We find a good coincidence between the envelopes of the Markov approximation and those of the FD simulations, which supports the reliability of the synthesis method using the Markov approximation. The envelopes of the Markov approximation are scaled by using a characteristic time, which is a function of propagation direction and other model parameters. It predicts that envelopes increase in duration and decrease in maximum amplitude more rapidly in the horizontal propagation than in the vertical when the media are characterized by long horizontal and short vertical correlation distances. In the case of the vertical wave propagation, the envelope of the anisotropic random media has shorter duration and larger maximum amplitude than those of the isotropic random media. It means that the intensity of the inhomogeneity is underestimated when one analyses seismogram envelopes of deep events considering anisotropic lithosphere as isotropic random media.

Key words: anisotropy, random media, scattering, seismic waves.

1 INTRODUCTION

The concept of random media, fluctuation from the average medium property is random in space, is widely accepted for modelling velocity inhomogeneity distributed from the very shallow crust to the upper mantle. The inhomogeneity at the very shallow crust can be directly measured in boreholes; fluctuations of *P*- and *S*-wave velocities can be considered as random (e.g. Shiomi *et al.* 1997), and are considered to be anisotropic with long horizontal and short vertical correlation distances (e.g. Wu *et al.* 1994; Dolan *et al.* 1998). Holliger & Levander (1992) reported the anisotropic inhomogeneity in the lower crust from a surface exposure at the Iverea Zone, Italy. Analyses of seismic array records also detect the anisotropic inhomogeneity in the lower crust (e.g. Hestholm *et al.* 1994; Matsumoto *et al.* 2001). Ryberg *et al.* (2000) employed the anisotropic random media in the upper mantle to explain the P_n-wave trains appearing in the observed seismograms of peaceful nuclear explosion. Furumura & Kennett (2005) distributed anisotropic inhomgeneity in the subducting plate to simulate regional seismograms observed in northern Japan. Kamei *et al.* (2005) proposed the anisotropic random media for modelling methane hydrate-bearing zones. In this study, we use the term 'anisotropic random media' to represent the random media where the characteristic scale length of the inhomogeniety depends on direction. It should be noted that some papers used the term 'anisomeric media' to distinguish the anisotropy of elastic tensor (e.g. Kravtsov *et al.* 2003). This study does not consider the anisotropy of the elastic tensor.

For interpretations of observed seismograms, it is useful to simulate wave propagation in anisotropic random media and to investigate its effects on wavefield. Iooss (1998) and Müller & Shapiro (2003) theoretically investigated traveltime and amplitude fluctuations in anisotropic random media on the bases of the Rytov method (e.g. Chernov 1960; Rytov *et al.* 1989). In those papers, they compared the theoretical

predictions using the Rytov method with those from finite-difference (FD) wave simulations, and found a good coincidence between them. Supposing the geometry of reflection seismic survey, Kravtsov *et al.* (2003) calculated traveltime fluctuation in anisotropic random media as a function of the incident angle. Scattered waves also strongly depend on the anisotropic inhomogeneity. Numerical simulations of wavefields with the FD method show that the anisotropy significantly affects the excitation of later phases (e.g. Ikelle *et al.* 1993). Jannaud *et al.* (1992) investigated coda-wave excitation in anisotropic random media on the basis of the single-back scattering model with the Born approximation; they also mentioned a possibility of the estimation of the anisotropy from coda-wave analysis.

Due to the wave scattering and the excitation of later phases, wave envelopes usually have long duration compared to source duration. Waves impulsively radiated from a source fluctuate due to the inhomogeneous media and the envelopes show increases in duration with travel distances. This is one of the prominent features of wave envelopes observed in inhomogeneous media. Using the parabolic approximation and the Markov approximation, we can theoretically synthesize wave envelopes without numerical wave propagation simulations (e.g. Ishimaru 1978; Sato & Fehler 1998). The method considers small-angle scattering around the forward direction and neglects large-angle scattering; small-angle scattering dominates over large-angle scattering when the characteristic scale of the inhomogeneity is larger than the wavelength. We refer to the envelopes synthesized by using the Markov approximation as Markov envelopes, hereinafter. Fehler *et al.* (2000) confirmed the validity of this method by comparing the Markov envelopes with the envelopes of wave traces from FD simulations in 2-D case. Sato (1989) first used the Markov envelopes to explain the increase of seismogram-envelope duration with travel distance, which is referred to as envelope broadening. Later, Saito *et al.* (2002) extended the method under more realistic assumptions. They explained not only envelope broadening but also maximum-amplitude decay of envelopes (Saito *et al.* 2005). Based on the envelope modelling, one can estimate the power spectral density function (PSDF) of velocity inhomogeneity in the lithosphere (e.g. Scherbaum & Sato 1991; Obara & Sato 1995). Also, one can roughly estimate the hypocentral distance analysing the initial part of a *P*-wave envelope observed at a single station (Tsukada *et al.* 2004). Recently, the Markov envelope was incorporated in the radiative transfer theory to simulate not only small-angle scattering but also large-angle scattering (Saito *et al.* 2003; Sato *et al.* 2004). Furthermore, Korn & Sato (2005) extended the Markov envelope to the elastic wave propagation case; they showed that the scalar-wave equation can be used for the envelope synthesis even in elastic media when the conversion scattering is negligibly small. We may say that the envelope modelling using the Markov approximation is one of the useful methods for interpreting seismogram envelopes. However, the conventional studies have supposed only isotropic inhomogeneity.

The present study formulates a method of scalar-wave envelope synthesis in anisotropic 2-D random media using the Markov approximation. In Section 2, we mention 2-D wave propagation in anisotropic random media and statistical characterization of the media. In Section 3, we numerically calculate the wave propagation with the FD method to obtain reference envelopes (FD envelopes) that will be compared with the Markov envelopes. In Section 4, the envelope synthesis method is formulated using the Markov approximation. We compare the Markov envelopes and the FD envelopes to examine the reliability of the theoretical calculations. In Section 5, we discuss the dependence of envelopes on the propagation direction in the anisotropic random media. Also, we compare the envelopes in anisotropic random media and those in isotropic random media. Finally, Section 6 presents some conclusions.

2 WAVE PROPAGATION IN 2-D ANISOTROPIC RANDOM MEDIA

Let us consider propagation of scalar wave $u(\boldsymbol{x}, t)$ through 2-D space governed by

$$\left(\Delta - \frac{1}{V(\boldsymbol{x})^2}\frac{\partial^2}{\partial t^2}\right)u(\boldsymbol{x}, t) = 0, \tag{1}$$

where $\boldsymbol{x} = (x, z)$ and Δ is the Laplacian in 2-D. In randomly inhomogeneous media, wave velocity is written as $V(\boldsymbol{x}) = V_0\{1 + \xi\,(\boldsymbol{x})\}$, where V_0 is the average velocity and ξ the fractional velocity fluctuation. Throughout this study, weak fluctuation $|\xi| \ll 1$ is assumed. To obtain statistical properties of the media and wavefield, we consider an ensemble of the fractional fluctuation $\{\xi(\boldsymbol{x})\}$ such that $\langle\xi(\boldsymbol{x})\rangle = 0$, where the angular brackets mean the ensemble average. The media are referred to as random media, which are statistically characterized by the autocorrelation function (ACF) of the fractional fluctuation $R(\boldsymbol{x}_d) \equiv \langle\xi(\boldsymbol{x}_d + \boldsymbol{x})\xi(\boldsymbol{x})\rangle$ or the power spectral density function (PSDF), $P(\boldsymbol{m})$, where $\boldsymbol{m}$ is the wavenumber. We suppose that ξ is statistically homogeneous random function in space; the ACF depends on difference vector $\boldsymbol{x}_d$ but is independent of location $\boldsymbol{x}$. The ACF and the PSDF are generally characterized by rms value of the fractional velocity fluctuation ε and two correlation distances a_x and a_z, which are the characteristic scale lengths of the inhomogeneity in the x and z directions, respectively.

A Gaussian ACF for 2-D anisotropic random media is given by

$$R(x_d, z_d) = \varepsilon^2 \exp\left(-\frac{{x_d}^2}{{a_x}^2} - \frac{{z_d}^2}{{a_z}^2}\right), \tag{2}$$

and the corresponding PSDF is given by

$$\begin{aligned} P(m_x, m_z) &= \int_{-\infty}^{\infty}\int_{-\infty}^{\infty} R\,(x_d, z_d)\exp\left(-im_x x_d - im_z z_d\right)\,dx_d\,dz_d \\ &= \varepsilon^2\pi a_x a_z \exp\left(-\frac{{a_x}^2{m_x}^2 + {a_z}^2{m_z}^2}{4}\right), \end{aligned} \tag{3}$$

where (m_x, m_z) is the wavenumber vector of the inhomogeneity. Fig. 1(a) shows an example of anisotropic random media characterized by the Gaussian ACF. In Fig. 1(b), an example of isotropic random media is also shown for comparison. The ACF and PSDF of the anisotropic

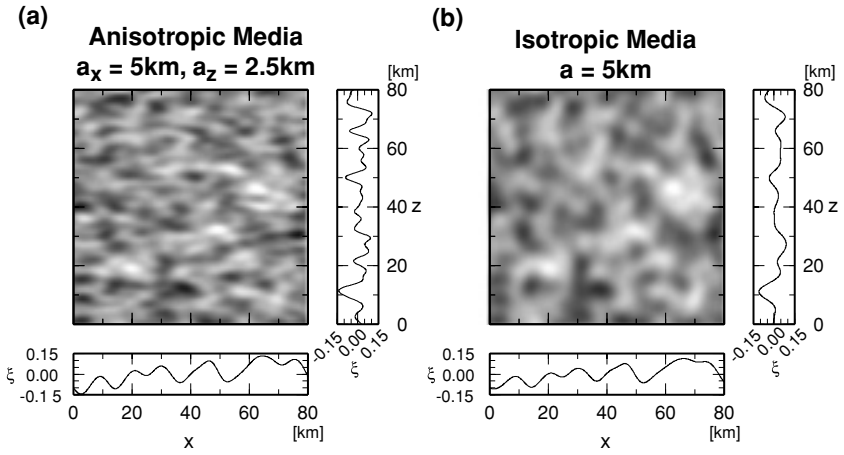

Figure 1. The random media characterized by the Gaussian autocorrelation function (ACF) with $\varepsilon = 0.05$. (a) Anisotropic random media with $a_x = 5$ km, $a_z = 2.5$ km and (b) isotropic random media with $a_x = a_z = 5$ km. The fractional velocity fluctuation is imaged by grey scale and the fluctuations along $x = 40$ km and $z = 40$ km are also plotted beside the image.

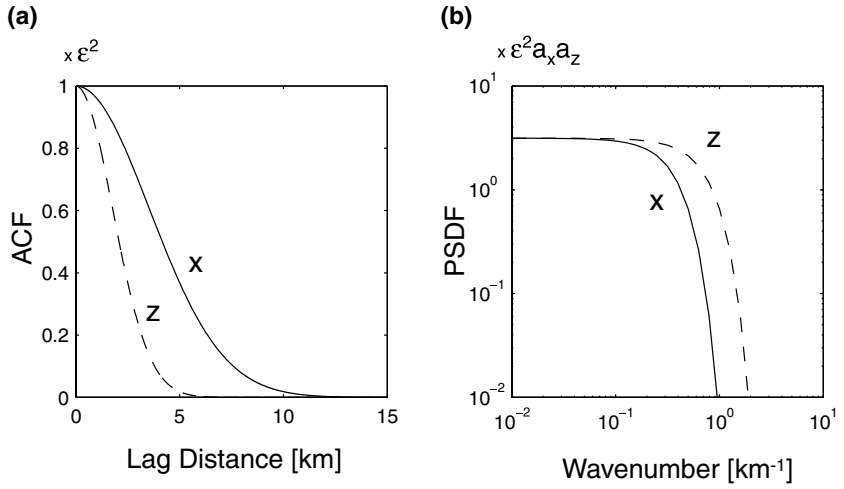

Figure 2. (a) The Gaussian ACF with $a_x = 5$ km and $a_z = 2.5$ km. A cross Section along x-axis is plotted by a solid curve and along z-axis by a dashed curve. (b) The corresponding power spectral density function (PSDF). A cross section along x-axis is plotted by a solid curve and along z-axis by a dashed curve.

random media are shown in Fig. 2. The correlation distances in the x- and z-axes are 5.0 and 2.5 km, respectively. The ACF decreases more rapidly in the z-axis than in the x-axis (Fig. 2a). The PSDF along the z-axis is richer in the short-wavelength components than that along the x-axis (Fig. 2b).

A von Kármán type ACF is given by

$$R(x_d, z_d) = \frac{\varepsilon^2 2^{1-\kappa}}{\Gamma(\kappa)} \left(\sqrt{(x_d/a_x)^2 + (z_d/a_z)^2}\right)^{\kappa} K_{\kappa}\left(\sqrt{(x_d/a_x)^2 + (z_d/a_z)^2}\right), \tag{4}$$

and the corresponding PSDF is given by

$$P(m_x, m_z) = \frac{4\pi\kappa\varepsilon^2 a_x a_z}{\left(1 + {a_x}^2 {m_x}^2 + {a_z}^2 {m_z}^2\right)^{\kappa+1}}, \tag{5}$$

where Γ and K_{κ} are the Gamma function and the modified Bessel function of the second kind of the order κ, respectively.

In general, the ACFs for 2-D anisotropic random media, including Gaussian and von Kármán type, can be represented by using a normalized ACF $\bar{R}(\bar{r})$,

$$R(x_d, z_d) = \varepsilon^2 \bar{R}\left(\sqrt{\frac{{x_d}^2}{{a_x}^2} + \frac{{z_d}^2}{{a_z}^2}}\right) = \varepsilon^2 \bar{R}(\bar{r}), \tag{6}$$

where the normalized difference distance is defined as

$$\bar{r} \equiv \sqrt{\frac{{x_d}^2}{{a_x}^2} + \frac{{z_d}^2}{{a_z}^2}}. \tag{7}$$

The corresponding PSDF in 2-D is given by

$$\begin{aligned} P(m_x, m_z) &= \int_{-\infty}^{\infty}\int_{-\infty}^{\infty} R(x_d, z_d)\exp(-im_x x_d - im_z z_d)\, dx_d\, dz_d \\ &= 2\pi\varepsilon^2 a_x a_z \int_0^{\infty} J_0(\bar{m}\bar{r})\bar{r}\,\bar{R}(\bar{r})\, d\bar{r} \\ &= \varepsilon^2 a_x a_z \bar{P}(\bar{m}), \end{aligned} \tag{8}$$

and J_0 is the Bessel function of zero order. The normalized PSDF is defined as

$$\bar{P}(\bar{m}) \equiv 2\pi \int_0^{\infty} J_0(\bar{m}\bar{r})\bar{r}\,\bar{R}(\bar{r})\, d\bar{r}, \tag{9}$$

where the normalized wavenumber is defined as

$$\bar{m} \equiv \sqrt{{a_x}^2 {m_x}^2 + {a_z}^2 {m_z}^2}. \tag{10}$$

Using the above expressions of the ACF (eq. 6) and PSDF (eq. 8) with the normalized functions, we can represent general type of 2-D anisotropic random media.

3 FD ENVELOPES IN 2-D ANISOTROPIC RANDOM MEDIA

Wave propagation in 2-D anisotropic random media is numerically simulated before the derivation of the Markov envelopes. Those numerical simulations would be helpful for intuitively recognizing wave propagation in anisotropic random media. Also, the envelopes obtained from the numerically calculated wavefield will be compared with the Markov envelopes in order to examine the reliability of the synthesis using the Markov approximation. We here consider the random media characterized by the Gaussian ACF with $\varepsilon = 0.05$, $a_x = 5.0$ km, $a_z = 2.5$ km and $V_0 = 4$ km s^{-1}. The orders of those values are consistent with the observed *S*-wave random inhomogeneity (e.g. Saito *et al.* 2005) and the parameters used in the previous works (e.g. Sato *et al.* 2004). The ratio $a_x/a_z = 2$ is consistent with that of the KTB borehole data obtained by Wu *et al.* (1994). In the medium with dimensions of 200 km square surrounded by absorbing boundaries, wave propagation from a point source with isotropic radiation is numerically simulated with the FD method. We use a Ricker wavelet with its dominant frequency $f_c = 2$ Hz as a source time function. The dominant frequency corresponds to $ka_x \approx 16$ and $ka_z \approx 8$ where k is the wavenumber given by $k = 2\pi f_c/V_0$. The FD simulations are accomplished with fourth-order accuracy in space and second-order in time with grid spacing of 50 m and time step of 4 ms.

To investigate statistical properties of wavefield, we make the above numerical simulations with respect to 50 realizations of the random media. As examples, Fig. 3 shows wave traces calculated by the FD simulations with respect to 3 realizations of the random media. The wave records after the arrival of reflected waves from the boundaries are excluded. Figs 3(a) and (b) show wave traces along the z- and x-axes, respectively. We consider Figs 3(a) and (b) as the vertical wave propagation and the horizontal propagation, respectively. Each row corresponds to each realization of the random media and the four panels in each row correspond to the distances, 50, 75, 100 and 125 km apart from the source. Wave traces, on the whole, become more complex with increasing propagation distance; later arrivals lengthen the duration of wave trains. This tendency is more prominent in the horizontal propagation cases, Fig. 3(b), than in the vertical propagation cases, Fig. 3(a).

From wave traces calculated with respect to 50 realizations of random media, we make mean-square (MS) envelopes and rms envelopes, as follows. We calculate 50 envelopes at each station by using the Hilbert transform (p. 250, Shearer 1999). At each station, squaring those 50 realized envelopes and averaging the squared envelopes, we obtain an ensemble-averaged squared envelope, which is referred to as MS envelope. Taking the square root of the MS envelope, we obtain rms envelope. The rms envelopes from FD simulations are referred to as FD envelopes, hereinafter. Fig. 4 shows the FD envelopes at stations located 50, 75, 100 and 125 km apart from the source. Each bin corresponds to each propagation direction ϕ; the directions, $\phi = 0$, 30, 45, 60 and 90 degree, are measured as the angle between the z-axis and the global ray direction. Solid black curves are the FD envelopes or ensemble-averaged envelopes made from 50 realized envelopes. Grey area around the solid curve indicates the range of standard deviation of the ensemble-averaged envelope. The range is estimated with bootstrap method; we estimate the standard deviation over 30 ensemble-averaged envelopes, which are calculated from artificial data sets. Each artificial data set consists of 40 envelopes, which are randomly sampled from the 50 realized envelopes. Fine grey curves indicate the standard deviation of the each realized envelope. Note that the large standard deviation of each realized envelope (fine grey curves in Fig. 4) means that the shapes of a single-realized envelope and the ensemble-averaged envelope are quite different. Although the standard deviation of each realized envelope is large, we see that the shape of the ensemble-averaged envelope is stable (grey areas in Fig. 4) when we use more than 40 realized envelopes for the average. In this study, we are interested in the ensemble-averaged envelope. The FD envelopes, or ensemble-averaged envelopes, increase in their duration and decrease in their maximum amplitude with increasing travel distance. This tendency is more prominent with increasing the angle ϕ.

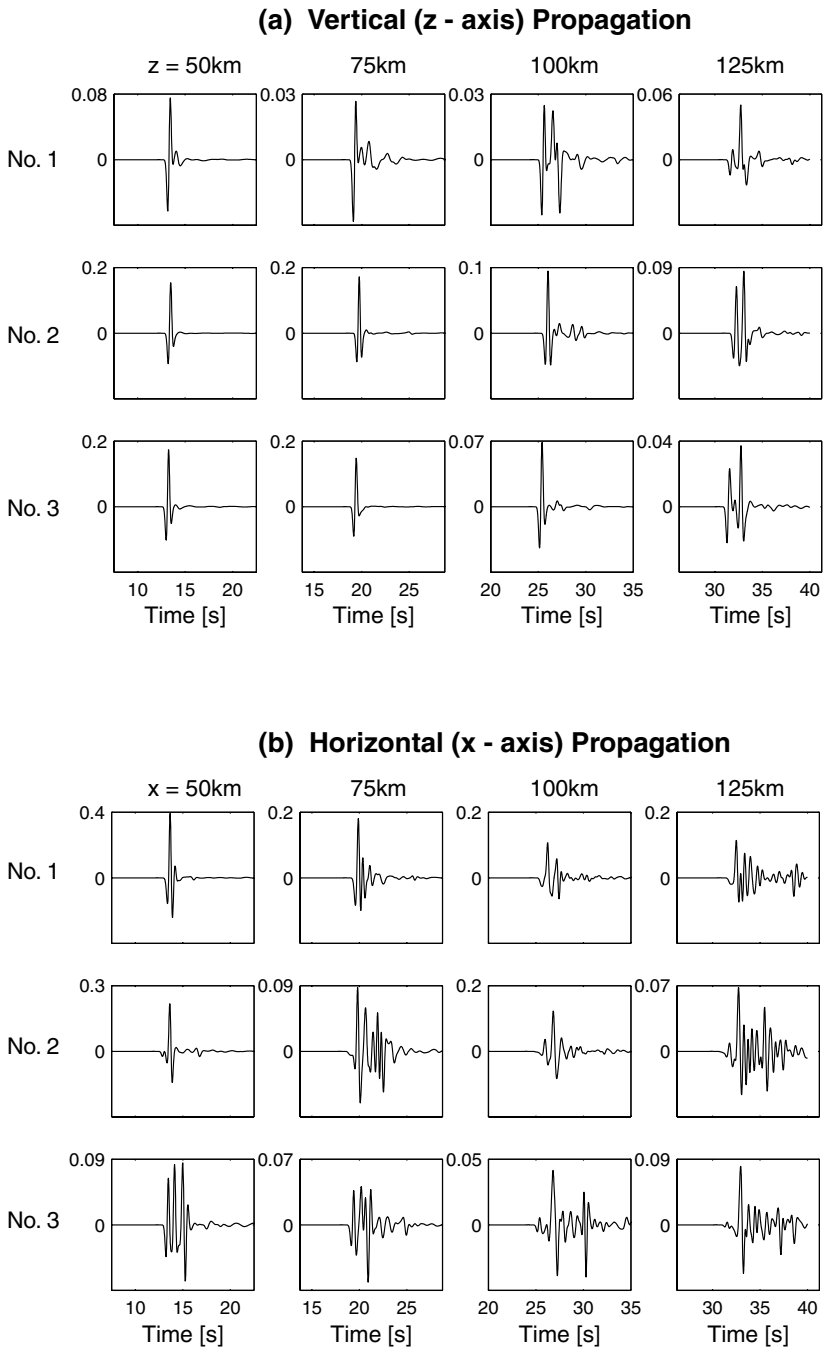

Figure 3. Wave traces calculated by the finite-difference simulations with respect to 3 realizations of random media characterized by the Gaussian ACF with $\varepsilon = 0.05$, $a_x = 5$ km, $a_z = 2.5$ km and $V_0 = 4$ km s^{-1}. (a) Wave traces at stations located at 50, 75, 100 and 125 km on the z-axis apart from a source. A set of four panels in each row is calculated for a single realization of the random media. (b) Wave traces at stations located at 50, 75, 100 and 125 km on the x-axis apart from a source.

4 MARKOV ENVELOPE IN 2-D RANDOM MEDIA

4.1 Formulation

4.1.1 General formulation for 2-D random media

Using 2-D polar coordinates (r, ϕ) shown in Fig. 5(a), we write wavefield as a superposition of harmonic cylindrical waves of angular frequency ω,

$$u(\mathbf{x}, t) = \frac{1}{2\pi} \int_{-\infty}^{\infty} \frac{U(r, \phi, \omega)}{\sqrt{kr}} \exp\{i(kr - \omega t)\}\, d\omega, \tag{11}$$

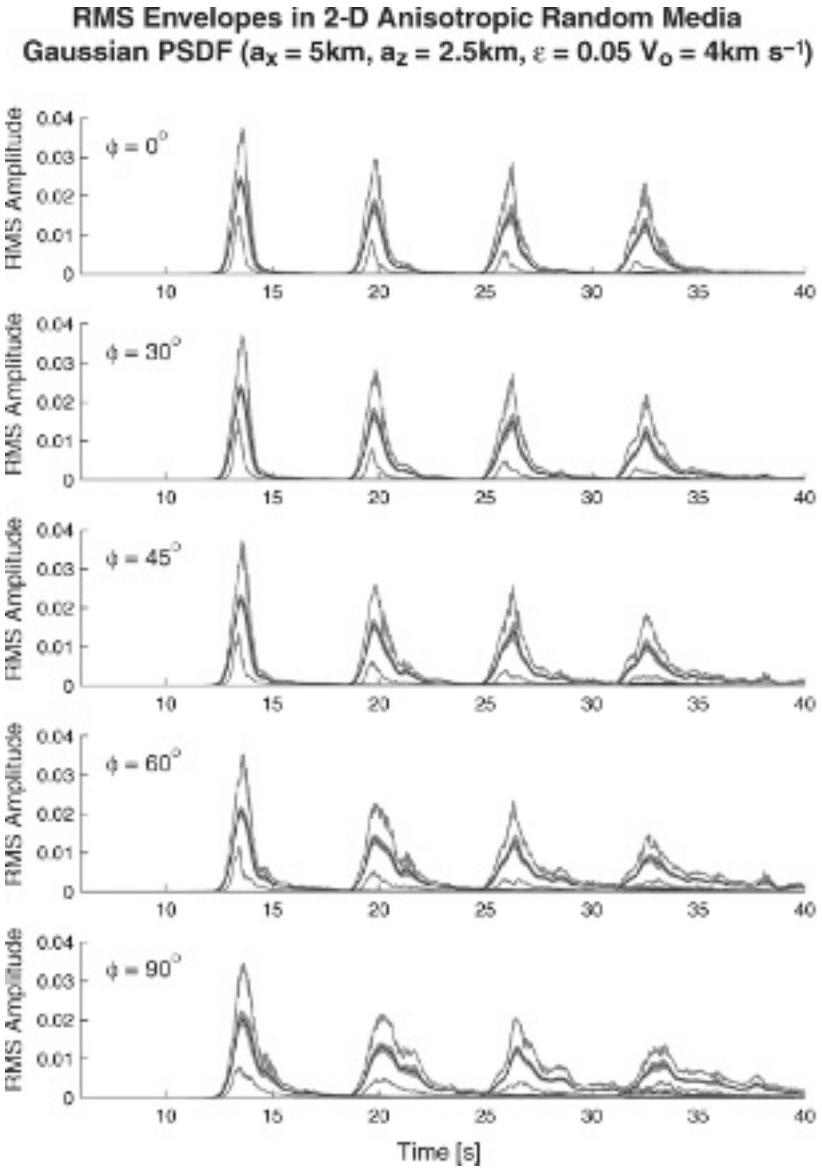

Figure 4. The rms envelopes of finite-difference wave simulations. The envelopes at travel distance 50, 75, 100 and 125 km are plotted. Numerals at upper left side in each bin show the propagation direction measured from the z-axis. Wave propagations from a 2 Hz Ricker wavelet source are numerically simulated for 50 realizations of the random media characterized by the Gaussian ACF with $\varepsilon = 0.05$, $a_x = 5$ km, $a_z = 2.5$ km and $V_0 = 4$ km s^{-1}. Solid black curves are the FD envelopes or ensemble-averaged envelopes over 50 realized envelopes. Grey area around the solid curve indicates the range of standard deviation of the FD envelope. Fine grey curves indicate the standard deviation of the each realized envelopes.

where the wavenumber $k = \omega/V_0$ (e.g. Saito *et al.* 2003). When the correlation distance of the medium inhomogeneity is much larger than the wavelength $ak \gg 1$, the second derivative of $U(r, \phi, \omega)$ with respect to radial direction r may be neglected. In addition, when wave travels much longer than the wavelength $rk \gg 1$, the parabolic wave equation is obtained from eqs (1) and (11),

$$2ik\frac{\partial}{\partial r}U(r,\phi,\omega) + \frac{1}{r^2}\frac{\partial^2}{\partial\phi^2}U(r,\phi,\omega) - 2k^2\xi(r,\phi)\,U(r,\phi,\omega) = 0. \tag{12}$$

For the case of $ak \gg 1$, small-angle scattering dominates. Hence, we consider wave propagation around the global ray direction ϕ. In Fig. 5(a), the angle ϕ_i is represented by small angle θ_i as $\phi_i = \theta_i + \phi$ where $|\theta_i| \ll 1$. Furthermore, a local coordinate $r_\perp$ is introduced at a large distance r from the source ($r \gg a$); the axis $r_\perp$, which is referred to as transverse axis, is tangential to the circle of radius r (Fig. 5a). In order to derive the envelopes, we introduce a two-frequency mutual coherence function (TFMCF) in the local coordinate. The TFMCF is defined at two adjacent points $r_{\perp 1}$ and $r_{\perp 2}$ on the transverse axis and two angular frequencies ω_1 and ω_2 as

$$\Gamma_2(r_{\perp 1}, r_{\perp 2}, r, \omega_1, \omega_2) \equiv \left\langle U(r_{\perp 1}, r, \omega_1)\, U^*(r_{\perp 2}, r, \omega_2)\right\rangle, \tag{13}$$

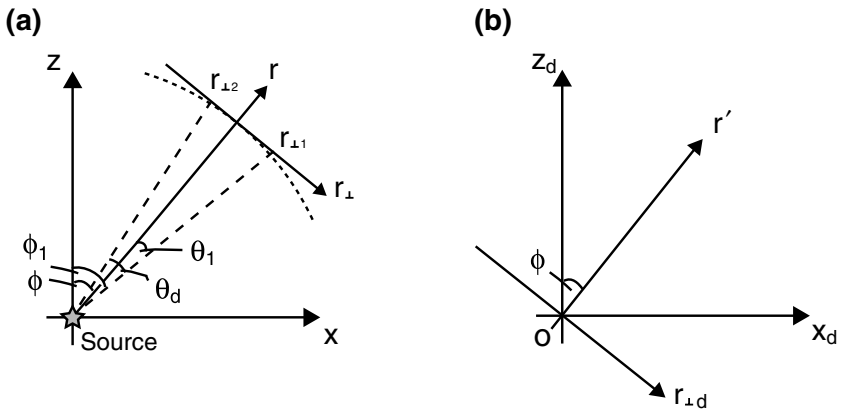

Figure 5. Coordinates used in the formulation of 2-D anisotropic media (x-z space). (a) The global ray direction from a source is in the radial direction r. A transverse axis $r_\perp$, which is tangential to the circle of radius r is taken at large distance r from the source. (b) Difference coordinates between two points $(r_{\perp 1}, r)$ and $(r_{\perp 2}, r)$; the origin is chosen at $(r_{\perp 2}, r)$. An axis r' is parallel to the global ray direction and an axis $r_{\perp d}$ is in the transverse axis $r_\perp$. Axes x_d and z_d are parallel to the axes x and z, respectively.

where asterisk denotes complex conjugate and $r_{\perp i} \approx r\theta_i$. The equation of Γ_2 is derived from eq. (12) as

$$2i\frac{\partial}{\partial r}\Gamma_2(r_{\perp 1}, r_{\perp 2}, r, \omega_1, \omega_2) + \frac{1}{r^2}\left(\frac{1}{k_1}\frac{\partial^2}{\partial {\phi_1}^2} - \frac{1}{k_2}\frac{\partial^2}{\partial {\phi_2}^2}\right)\Gamma_2 \\ -2\left\langle\{k_1\xi(r_{\perp 1}, r) - k_2\xi(r_{\perp 2}, r)\}U(r_{\perp 1}, r, \omega_1)U^*(r_{\perp 2}, r, \omega_2)\right\rangle = 0. \tag{14}$$

When we consider the range such that $|r_{\perp 1} - r_{\perp 2}| \ll r$ in homogeneous random media, Γ_2 strongly depends on the difference angle $\theta_d \equiv \theta_1 - \theta_2$, while it is almost independent of the centre of mass coordinate $\theta_c \equiv (\theta_1 + \theta_2)/2$ within the local coordinates. Hence, the derivatives with respect to angles ϕ_i are approximated as $\partial^2/\partial\phi_1^2 \approx \partial^2/\partial\phi_2^2 \approx \partial^2/\partial\theta_d^2$. Considering the two points $(r_{\perp 1}, r)$ and $(r_{\perp 2}, r)$ on the transverse axis, we introduce difference coordinates $x_d = x_1 - x_2$ and $z_d = z_1 - z_2$ at distance r where x_i and z_i indicate the position of $(r_{\perp i}, r)$ in the x-z coordinates (Figs 5a and b). Introducing difference coordinates $(r_{\perp d}, r')$, where the $r_{\perp d}$-axis is parallel to the $r_\perp$-axis and the r'-axis is parallel to the r-axis, we define the longitudinal integral of the ACF along the global ray direction as

$$A(r_{\perp d}, \phi) \equiv \int_{-\infty}^{\infty} R(\boldsymbol{x_d})dr' = \frac{1}{(2\pi)^2}\int_{-\infty}^{\infty}dr'\int_{-\infty}^{\infty}\int_{-\infty}^{\infty} P(\boldsymbol{m})\exp\{i\boldsymbol{m}\cdot\boldsymbol{x_d}\}\,d\boldsymbol{m} \\ = \frac{1}{(2\pi)^2}\int_{-\infty}^{\infty}dr'\int_{-\infty}^{\infty}\int_{-\infty}^{\infty} P(\boldsymbol{m})\exp\{i\boldsymbol{m}\cdot(r_{\perp d}\boldsymbol{e}_\perp + r'\boldsymbol{e}_r)\}d\boldsymbol{m}, \tag{15}$$

where $r_{\perp d} = r_{\perp 1} - r_{\perp 2}$, the vectors $\boldsymbol{e_r}$ and $\boldsymbol{e}_\perp$ are unit vectors in the r'- and $r_{\perp d}$-axes, respectively. The difference vector $\boldsymbol{x_d} = (x_1 - x_2, z_1 - z_2)$ is given by $\boldsymbol{x_d} = r_{\perp d}\,\boldsymbol{e}_\perp + r'\,\boldsymbol{e_r}$. The third term in eq. (14) is approximated as

$$\left\langle(k_1\xi_1 - k_2\xi_2)\,U_1U_2^*\right\rangle \approx -\frac{i}{2}\left[\left({k_1}^2 + {k_2}^2\right)A(0, \phi) - 2k_1k_2A(r_{\perp d}, \phi)\right]\Gamma_2, \tag{16}$$

where U_i means that its argument is $(r_{\perp i}, r, \omega_i)$ and ξ_i means that its argument is $(r_{\perp i}, r)$ (see Appendix A). During the derivation, large-angle scattering, or backward scattering, is neglected. Also, we suppose weak anisotropy and the existence of an intermediate scale Δr, which is larger than the correlation distance of inhomogeneity but smaller than the scale of variation of U. The approximation is called the Markov approximation (e.g. Sato & Fehler 1998). From eqs (14) and (16), the master equation of the TFMCF, for quasi-monochromatic waves $\omega_1 \approx \omega_2$, is written as

$$\frac{\partial}{\partial r}\Gamma_2(\theta_d, r, \omega_c, \omega_d; \phi) + i\frac{k_d}{2{k_c}^2}\frac{1}{r^2}\frac{\partial^2}{\partial {\theta_d}^2}\Gamma_2 + {k_c}^2\left[A(0, \phi) - A(r\,\theta_d, \phi)\right]\Gamma_2 + \frac{{k_d}^2}{2}A(0, \phi) = 0, \tag{17}$$

where we use $r_{\perp d} \approx r\theta_d$. Also, the centre of mass and the difference wavenumbers are $k_c = (k_1 + k_2)/2$ and $k_d = k_1 - k_2$, respectively. Corresponding coordinates for the angular frequency are also used. We introduced ${}_0\Gamma_2$ as $\Gamma_2 = {}_0\Gamma_2\,\exp\{-{k_d}^2A(0, \phi)r/2\}$ The term $\exp\{-{k_d}^2A(0, \phi)\,r/2\}$ is referred to as the wandering effect term, which corresponds to the travel time fluctuation over each realization of the envelopes (e.g. Lee & Jokipii 1975b). From eq. (17), we obtain the master equation for ${}_0\Gamma_2$ as,

$$\frac{\partial}{\partial r}{}_0\Gamma_2(\theta_d, r, \omega_c, \omega_d; \phi) + i\frac{k_d}{2{k_c}^2}\frac{1}{r^2}\frac{\partial^2}{\partial {\theta_d}^2}{}_0\Gamma_2 + {k_c}^2\left[A(0, \phi) - A(r\,\theta_d, \phi)\right]{}_0\Gamma_2 = 0. \tag{18}$$

The squared envelope in a narrow-frequency band $\Delta\omega_c$ around the centre angular frequency ω_c is written as

$$I(r, t, \omega_c, \phi) \equiv \langle|u|^2\rangle \\ \approx \frac{\Delta\omega_c}{(2\pi)^2k_cr}\int_{\omega_c-\Delta\omega_c/2}^{\omega_c+\Delta\omega_c/2}{}_0\Gamma_2(\theta_d = 0, r, \omega_d, \omega_c; \phi)\exp\{-i\omega_d(t - r/V_0)\}d\omega_d. \tag{19}$$

By solving the master equation of TFMCF (18) and inserting the solved TFMCF into eq. (19), we can synthesize the MS envelope without the wandering effect. Square root of the MS envelope is the rms envelope. We refer to the rms envelope derived from the Markov approximation as Markov envelope, hereinafter.

4.1.2 Anisotropic random media

We derive the master equation of TFMCF and the Markov envelope in the case of anisotropic random media. From Fig. 5(b), the relation between (x_d, z_d) and $(r_{\perp d}, r')$ is given by

$$x_d = r_{\perp d}\cos\phi + r'\sin\phi \quad \text{and} \quad z_d = -r_{\perp d}\sin\phi + r'\cos\phi. \tag{20}$$

Using eq. (20), we calculate eq. (15) as

$$\begin{aligned} A(r_{\perp d}, \phi) &\equiv \int_{-\infty}^{\infty} R(x_d, z_d)\, dr' \\ &= \int_{-\infty}^{\infty} dr' \frac{1}{(2\pi)^2} \int_{-\infty}^{\infty}\int_{-\infty}^{\infty} P(m_x, m_z)\exp(i m_x x_d + i m_z z_d)\, dm_x\, dm_z \\ &= \frac{1}{(2\pi)^2} \int_{-\infty}^{\infty} dr' \int_{-\infty}^{\infty}\int_{-\infty}^{\infty} P(m_x(m_r, m_\perp, \phi), m_z(m_r, m_\perp, \phi)) \times \exp(i m_r r' + i m_\perp r_{\perp d})\, dm_r dm_\perp \\ &= \frac{1}{2\pi} \int_{-\infty}^{\infty} P\,(m_x(m_r = 0, m_\perp, \phi), m_z(m_r = 0, m_\perp, \phi))\exp(i m_\perp r_{\perp d})\, dm_\perp, \end{aligned} \tag{21}$$

where

$$m_\perp \equiv m_x\cos\phi - m_z\sin\phi \quad \text{and} \quad m_r \equiv m_x\sin\phi + m_z\cos\phi. \tag{22}$$

Substituting eq. (8) into eq. (21) and considering the coefficient of $m_\perp$ in the PSDF as an correlation distance a_t along the $r_{\perp d}$-axis, we obtain

$$\begin{aligned} A(r_{\perp d}, \phi) &= \frac{1}{2\pi}\varepsilon^2 a_x a_z \int_{-\infty}^{\infty} \bar{P}(a_t m_\perp)\exp(i m_\perp r_{\perp d}) dm_\perp \\ &= \frac{1}{2\pi}\varepsilon^2 a_r \int_{-\infty}^{\infty} \bar{P}(\bar{m}_\perp)\exp(i\bar{m}_\perp r_{\perp d}/a_t) d\bar{m}_\perp, \end{aligned} \tag{23}$$

with the normalized PSDF (eq. 9) where $\bar{m}_\perp \equiv a_t m_\perp$. Here, the values of a_t and a_r are effective correlation distances in the $r_\perp$- and r-axes, which are defined as

$$a_t \equiv \sqrt{{a_x}^2\cos^2\phi + {a_z}^2\sin^2\phi} \quad \text{and} \quad a_r \equiv a_x a_z/\sqrt{{a_x}^2\cos^2\phi + {a_z}^2\sin^2\phi}, \tag{24}$$

respectively. The effective correlation distances are the functions of the angle ϕ; $a_t = a_x$ and $a_r = a_z$ when $\phi = 0$, and $a_t = a_z$ and $a_r = a_x$ when $\phi = \pi/2$.

The non-dimensional PSDF's of the Gaussian and von Kármán-type ACFs are given by

$$\bar{P}(\bar{m}) = \begin{cases} \pi\exp\left(-\bar{m}^2/4\right) & \text{Gaussian.} \\ \dfrac{4\pi\kappa}{(1+\bar{m}^2)^{\kappa+1}}, \quad \kappa > 0 & \text{von Karman.} \end{cases} \tag{25}$$

For the case of the Gaussian ACF, eq. (23) is given by

$$A(r_{\perp d}, \phi) = \sqrt{\pi}\varepsilon^2 a_r \exp\left(-\frac{{r_{\perp d}}^2}{{a_t}^2}\right). \tag{26}$$

At a long distance from the source, the correlation of the wavefield at two points spatially separated on the transverse axis rapidly decreases to zero with increasing the lag distance (see p. 245, Sato & Fehler 1998). Hence, the value of $A(0, \phi) - A(r_{\perp d}, \phi)$ at small transverse distance $r_{\perp d} \ll a_t$ is dominant in eq. (18). The value is approximated as

$$A(0, \phi) - A(r_{\perp d}, \phi) \approx \sqrt{\pi}\varepsilon^2 a_r \left(\frac{r_{\perp d}}{a_t}\right)^2. \tag{27}$$

For the case of the von Kármán type ACF, eq. (23) is given by

$$A(r_{\perp d}, \phi) = \frac{2^{3/2-\kappa}\sqrt{\pi}\varepsilon^2 a_r}{\Gamma(\kappa+1)} \left(\frac{r_{\perp d}}{a_t}\right)^{\kappa+1/2} K_{\kappa+1/2}\left(\frac{r_{\perp d}}{a_t}\right), \tag{28}$$

and the value of $A(0, \phi) - A(r_{\perp d}, \phi)$ is approximated as

$$A(0, \phi) - A(r_{\perp d}, \phi) \approx C(\kappa)\,\varepsilon^2 a_r \left(\frac{r_{\perp d}}{a_t}\right)^{p(\kappa)}, \tag{29}$$

where $C(\kappa)$ and $p(\kappa)$ are numerically calculated in Saito *et al.* (2002). From eqs (27), (29) and (18), the master equation of TFMCF is given by

Table 1. Parameters C and p for different type of random media.

Random media type	C	p
Gaussian ACF	$\sqrt{\pi}$	2
κ (von Kármán-type ACF)		
0.1	0.56	1.19
0.2	1.06	1.38
0.3	1.56	1.56
0.4	2.00	1.71
0.5	2.28	1.83
0.6	2.31	1.91
0.7	2.14	1.95
0.8	1.90	1.98
0.9	1.68	1.99
1.0	1.50	1.99

$$\frac{\partial}{\partial r}{}_0\Gamma_2(\theta_d, r, \omega_c, \omega_d; \phi) + i\frac{k_d}{2{k_c}^2}\frac{1}{r^2}\frac{\partial^2}{\partial {\theta_d}^2}{}_0\Gamma_2 + {k_c}^2 C\varepsilon^2 a_r\left(\frac{r\theta_d}{a_t}\right)^p {}_0\Gamma_2 = 0, \tag{30}$$

for the cases of the Gaussian and von Kármán-type ACFs. The values of C and p depend on the type of random media. For the Gaussian ACF, $p = 2$ and $C = \sqrt{\pi}$. For the von Kármán-type ACF, the values of C and p depend on the order κ (Table 1). Eq. (30) is the same as that in isotropic random media except the use of a_t and a_r (Fehler *et al.* 2000; Saito *et al.* 2003; Sato *et al.* 2004). Introducing the characteristic time for angular frequency ω_c at travel distance r_0 as

$$t_M \equiv \frac{V_0 r_0}{2{\omega_c}^2 {a_t}^2}\left(\frac{C\varepsilon^2{\omega_c}^2 a_r r_0}{V_0^2}\right)^{2/p}, \tag{31}$$

and the non-dimensional travel distance and difference angle as,

$$\tau \equiv r/r_0 \ \text{ and } \ \chi \equiv \sqrt{2r_0{\omega_c}^2 t_M/V_0}\,\theta_d, \tag{32}$$

respectively, we rewrite eq. (30) as

$$\frac{\partial}{\partial\tau}{}_0\Gamma_2 + it_M\omega_d\frac{1}{\tau^2}\frac{\partial^2}{\partial\chi^2}{}_0\Gamma_2 + \tau^p\chi^p{}_0\Gamma_2 = 0. \tag{33}$$

When $p = 2$, we can use the analytic solution of ${}_0\Gamma_2$ derived by Fehler *et al.* (2000) since eq. (33) is the same as eq. (30) in Fehler *et al.* (2000). When $p \neq 2$, we numerically solve eq. (33) with the FD method (see Saito et el. 2002). Inserting the solved ${}_0\Gamma_2$ into eq. (19), we can obtain squared-amplitude Markov envelopes without the wandering effect. Here, we consider the case of an isotropic source radiation of the delta-function source time function, $I(r \to 0) = 1/(2\pi r)\,\delta(t - r/V_0)$. For the corresponding conditions, we take ${}_0\Gamma_2$ to be ${}_0\Gamma_2 = k_c/\Delta\omega_c$, and suppose the integration range of ω_d in eq. (19) to be infinity at the source, $r = 0$. In practice, the integration range of ω_d is finite at a travel distance r since ${}_0\Gamma_2$ decreases to zero with increasing ω_d. Fig. 6 plots the squared-amplitude Markov envelopes for the radiation condition $I(r \to 0) = 1/(2\pi r)\,\delta(t - r/V_0)$, where the square amplitude is normalized by the geometrical spreading factor and the characteristic time (eq. 31), and the reduced time is normalized by the characteristic time. We may consider the characteristic time as the duration time of the envelopes. As the characteristic time increases, the duration increases and the amplitude decreases.

4.1.3 Validity range of the Markov envelopes

When we derive eqs (12) and (16), we assume small-angle scattering around the forward direction and neglect large-angle scattering. We evaluate the large-angle scattering to discuss the validity range of the Markov envelopes as follows. By using the Born approximation, the scattering coefficient in 2-D anisotropic random media is calculated as a function of scattering angle θ for the case of incident angle ϕ measured from the z-axis (Jannaud *et al.* 1992):

$$g(\theta) = \varepsilon^2 k^3 a_x a_z \bar{P}(\bar{k}), \tag{34}$$

where

$$\bar{k}^2 = k^2 a_x^2\{\sin(\theta+\phi) - \sin\phi\}^2 + k^2 a_z^2\{\cos(\theta+\phi) - \cos\phi\}^2. \tag{35}$$

It should be noted that the scattering coefficient (eq. 34) is not always a symmetric function with respect to θ, while that of isotropic random media is a symmetric function. Using a cut-off angle θ_c, we introduce a value:

$$r_0 g_L \equiv r_0\frac{1}{2\pi}\int_{|\theta|>\theta_c} g(\theta)\,d\theta = \varepsilon^2(r_0 k)(ka_x)(ka_z)\frac{1}{2\pi}\int_{|\theta|>\theta_c}\bar{P}(\bar{k}(\theta))\,d\theta, \tag{36}$$

as a measure of large-angle scattering. This value is related to the scattering attenuation for the main part of envelope, or around the maximum amplitude, at travel distance r_0 (Sato 1982; Wu 1982). Also, the value is related to coda-wave excitation since the attenuated wave energy

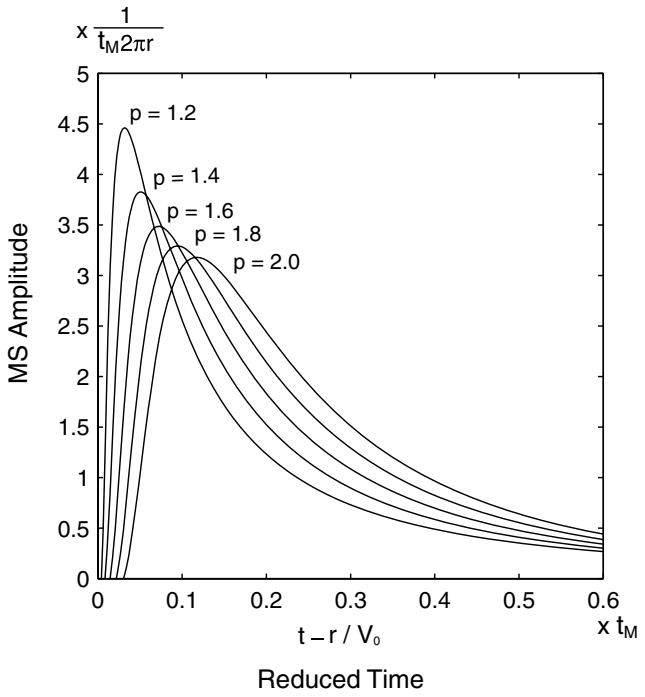

Figure 6. Theoretical mean-square (MS) envelopes in 2-D random media calculated by using the Markov approximation. Square amplitude is scaled by using the characteristic time t_M and geometrical spreading factor. Reduced time is scaled by t_M. The value of p depends on the type of random media. For the Gaussian ACF, $p = 2$. For the von Kármán-type ACF, the value of p is a function of the order κ (see Table 1).

appears again as coda-wave energy. Hence, the value of eq. (36) would be one of the appropriate parameters for judging the applicability of the envelope synthesis using the small-angle scattering approximation. When $r_0 g_L \ll 1$, we may consider that the effects of the large-angle scattering are small enough within travel distance r_0. On the value of the cut-off angle θ_c, we have no consensus at present. Recently, Kawahara (2002) theoretically predicted $\theta_c \approx 65^\circ$ by using the Kramers-Krönig relation (e.g. Aki & Richards 1980). On the other hand, this study uses $\theta_c = 30^\circ$ referring to Sato (1982) since the case of $\theta_c = 30^\circ$ predicting larger g_L than $\theta_c = 65^\circ$ is preferable for judging the condition $r_0 g_L \ll 1$. It should be noted that the condition $r_0 g_L \ll 1$ would be satisfied when $ka_x \gg 1$ and $ka_z \gg 1$ for the case of the Gaussian ACF since the order of $\bar{k}$ is the same as ka_x and ka_z.

Another limitation of the Markov envelope would come from the approximation used in eq. (16); we suppose the existence of an intermediate scale Δr, which is larger than the correlation distance in r-axis, but smaller than the scale of the wavefield variation in the r-axis (see p. 243 and 246, Sato & Fehler 1998). It is difficult to discuss the existence of Δr quantitatively. However, we expect that the existence of the intermediate scale Δr would be easily assured for the wave propagation along the z-axis when $a_x > a_z$ since the correlation distance a_z is small. On the other hand, when the anisotropy is strong $a_x \gg a_z$, the existence of Δr would not always be assured for the wave propagation along the x-axis.

4.2 Comparisons between Markov envelopes and FD envelopes

For the FD envelopes plotted in Fig. 4, the condition (eq. 36) is satisfied; the values of $r_0 g_L$ with $\theta_c = 30$ degree are estimated as the order of 10^{-7}, 10^{-5}, 10^{-3}, 10^{-2} and 10^{-2} for the angles $\phi = 0$, 30, 45, 60 and 90 degree, respectively. In those cases, the Markov envelopes are expected to be synthesized properly. In Fig. 7, the Markov envelopes are plotted by solid black curves, where the Markov envelopes in different incident angles are calculated with the same source radiation energy. The Markov envelopes are convoluted with the wandering effect, in other words, Γ_2 is used instead of ${}_0\Gamma_2$. Additionally, the temporal change in the power of a 2 Hz Ricker wavelet is convoluted with the MS envelopes since the Ricker wavelet is used as the source time function in the FD simulations. The Markov envelopes (solid curves) are in good agreement with the FD envelopes (grey curves) for all the travel distances for all the incident angles. This supports the reliability of the envelope synthesis using the Markov approximation. There are some slight discrepancies. As example, for the envelopes at the distance $r =$ 75 km with the incident angle $\phi = 60$ degree, the later phase excitation of the FD envelope at the time around 22 s cannot be explained by the Markov envelope. Such larger later-phase excitation in the FD envelopes would be caused by large-angle scattering, which is neglected in the formulation of the Markov envelope.

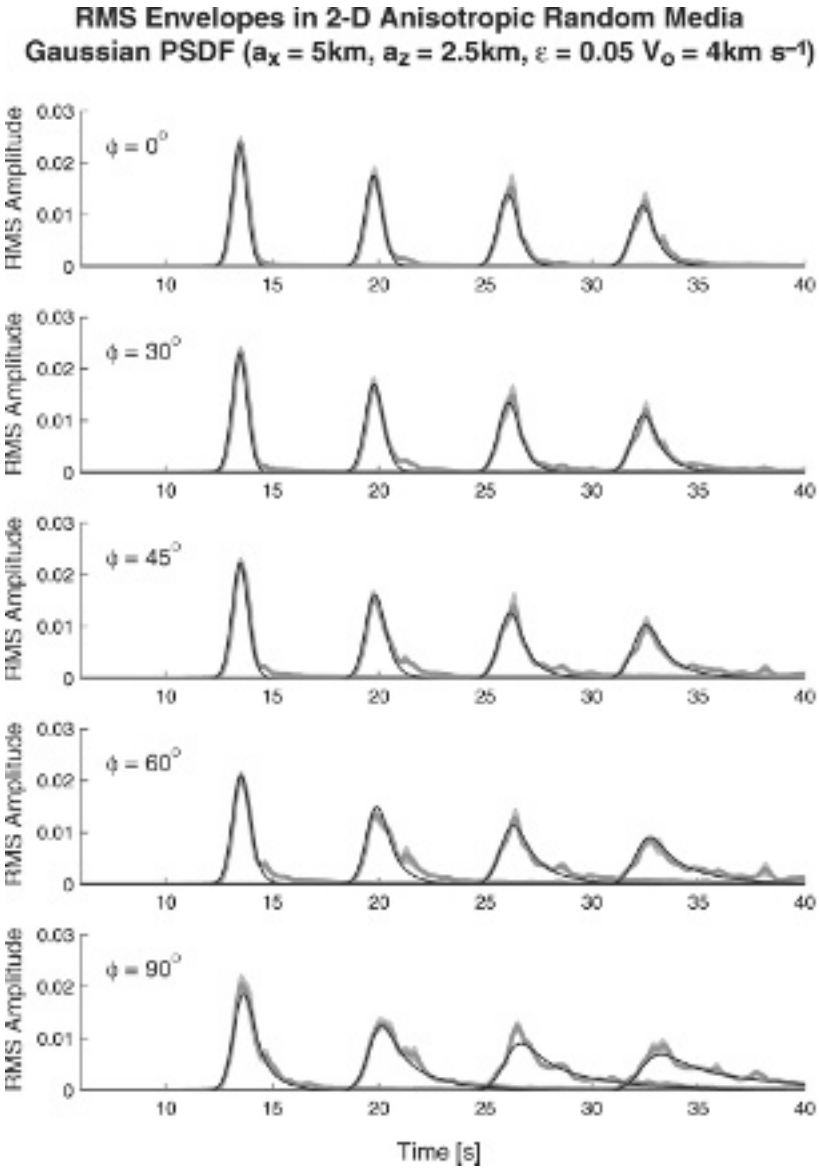

Figure 7. The rms envelopes for a 2 Hz Ricker wavelet source in 2-D random media characterized by the Gaussian ACF with $\varepsilon = 0.05$, $a_x = 5$ km, $a_z = 2.5$ km and $V_0 = 4$ km s^{-1}. The envelopes at travel distance 50, 75, 100 and 125 km are plotted. Numerals at upper left side in each bin show incident angle measured from the z-axis. Solid-black curves show rms envelopes based on the Markov approximation (Markov envelopes) Bold-grey curves and grey areas around the curves show rms envelopes by FD simulations (FD envelopes) and their standard deviations, respectively.

5 DISCUSSION

5.1 Dependence of wave propagation on the propagation direction

The characteristic time t_M (eq. 31), which can be considered as the envelope duration or a measure for distortion of envelopes, is almost the same as that of isotropic random media (see eq. 16 in Sato *et al.* 2004). Incident-angle dependence is additionally included in eq. (31) through the effective correlation distances, a_t and a_r. Fig. 8(a) shows the effective correlation distances (eq. 24) against the incident angle ϕ. As the incident angle changes from $\phi = 0$ to $\phi = \pi/2$, a_t changes from a_x to a_z and a_r changes from a_z to a_x. Fig. 8(b) shows the traveltime fluctuation at a travel distance $r = 200$ km for the Gaussian ACF with $\varepsilon = 0.05$, $a_x = 5$ km, $a_z = 2.5$ km and $V_0 = 4$ km s^{-1}. This is calculated on the basis of the geometrical optic approximation (p. 234, Sato & Fehler 1998) as

$$\sqrt{\left\langle \left(\int_0^r \frac{dr'}{V(\mathbf{x})} - \frac{r}{V_0} \right)^2 \right\rangle} = \frac{\sqrt{r\,A(0,\phi)}}{V_0}. \tag{37}$$

It should be noted that the geometrical optic approximation does not include the finite-wavelength effect on the traveltime fluctuation. The traveltime fluctuation increases with increasing the incident angle. When wave propagates along the x-axis ($\phi = \pi/2$), the traveltime fluctuation

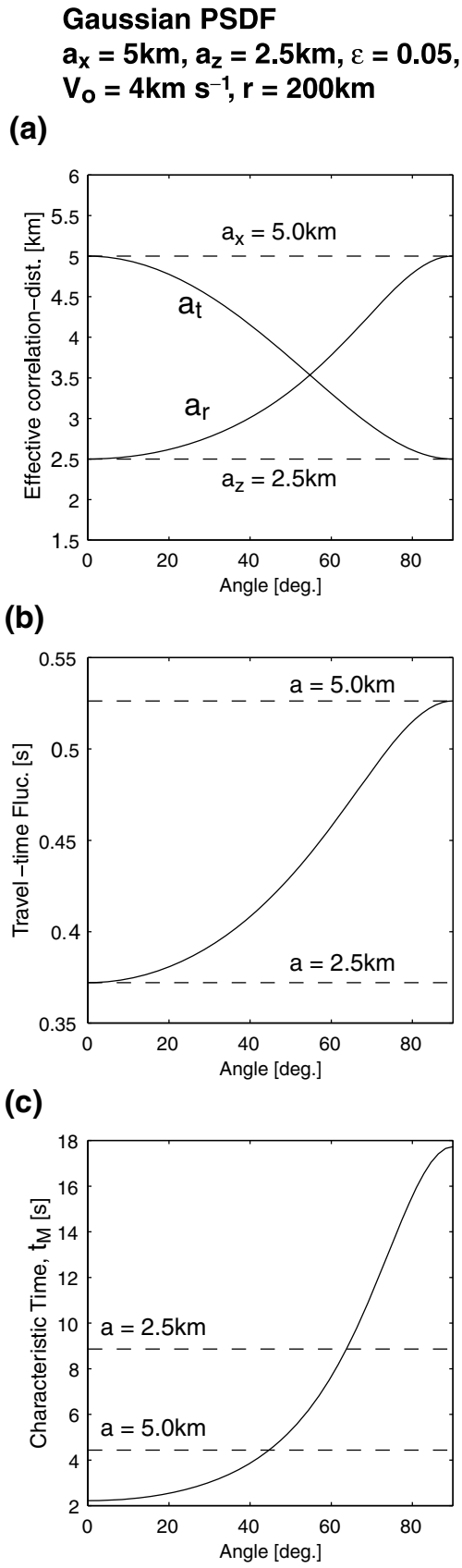

Figure 8. Incident angle dependence of (a) effective correlation distances a_t and a_r, (b) traveltime fluctuation predicted by the geometrical optics (eq. 37) and (c) characteristic time (eq. 31). Those values are calculated at travel distance of 200 km in the random media characterized by the Gaussian ACF with $\varepsilon = 0.05$, $a_x = 5$ km, $a_z = 2.5$ km and $V_0 = 4$ km s^{-1}. Broken lines show the values in the case of isotropic random media with $a_x = a_z = 5$ km and 2.5 km.

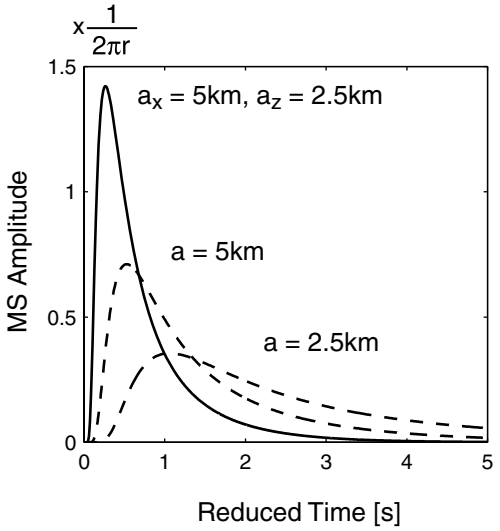

Figure 9. Squared-amplitude Markov envelopes at travel distance of 200 km for vertical (along the z-axis) wave propagation through 2-D random media characterized by the Gaussian ACF with $\varepsilon = 0.05$. The envelope in anisotropic media with $a_x = 5$ and $a_z = 2.5$ km is plotted by a solid curve. The envelopes in isotropic media with $a_x = a_z = 5$ and 2.5 km by dashed curves.

takes the maximum value, which is the same as that calculated from the isotropic random media of a correlation distance a_x. The traveltime fluctuation at $\phi = 0$ is the same as that from the isotropic random media of a correlation distance a_z. This behaviour is easily predicted since the value of $A(0, \phi)$ is proportional to a_r (see eq. 23). Fig. 8(c) shows the characteristic time (eq. 31) against the incident angle. The characteristic time also increases with increasing the incident angle. However, the behaviour is not so simple as the traveltime fluctuation predicted by the geometrical optic approximation; neither of the minimum value of t_M nor the maximum value corresponds to that predicted from the isotropic random media. It is because that t_M is proportional to a combination of the effective correlation distances; the combination is given by $a_r/a_t{}^2$ for the case of the Gaussian ACF. This makes the variation range of t_M wider than the range calculated from the isotropic random media of correlation distance a_x and a_z.

5.2 Envelopes in anisotropic lithosphere

Fig. 9 shows squared-amplitude Markov envelopes in anisotropic random media and isotropic random media for the case of vertical wave incidence ($\phi = 0$ in Fig. 8). The envelope of the anisotropic random media has larger maximum amplitude and shorter duration than those of the isotropic random media with a correlation distance a_x or a_z. This discrepancy between the anisotropic and isotropic cases causes serious problems when estimating the random inhomogeneity from observed seismogram envelopes. We shall consider a case as follows. One analyses wave envelopes of the vertical wave incidence, or of deep events, to estimate the random inhomogeneity assuming isotropic random media, even though those envelopes actually propagate through anisotropic random media. The estimated correlation distance of isotropic random media would be larger than a_x and a_z. In other words, one would underestimate the spectral amplitude of the inhomogeneity. Analysing seismogram envelopes of the intermediate-depth events on the basis of the Markov envelopes of isotropic random media, Saito *et al.* (2005) estimated the PSDF of the inhomogeneous lithosphere in northeastern Honshu, Japan. They discussed that the estimated PSDF would not give enough coda excitation observed in past studies. The anisotropic inhomogeneity in the lithosphere may be one of the keys to solve this discrepancy. Although this study is limited to 2-D case, the formulation for the 3-D case is necessary for more rigorous and quantitative discussions of the anisotropic lithosphere.

6 CONCLUSIONS

The present study formulates a method of envelope synthesis using the Markov approximation in 2-D weakly anisotropic random media characterized by the Gaussian and von Kármán-type ACFs. The reliability of the formulation is examined by FD numerical simulations; wave propagation of a 2 Hz Ricker wavelet source through the random media characterized by the Gaussian ACF with $\varepsilon = 0.05$, $a_x = 5$ km, $a_z = 2.5$ km and $V_0 = 4$ km s^{-1} is numerically solved in the travel distance ranging from 50 to 125 km. The envelopes of the Markov approximation are in good agreement with the envelopes obtained from wave traces of the FD simulations. This supports the reliability of the envelope synthesis using the Markov approximation. As in the case of isotropic random media, the Markov envelopes are scaled by using the characteristic time. The characteristic time is represented as a function of the propagation direction, the travel distance, the wave frequency and the parameters of random media. It predicts that envelopes increase in duration and decrease in maximum amplitude more rapidly in the horizontal propagation than in the vertical when the media are characterized by long horizontal and short vertical correlation distances.

Especially, in the case of the vertical wave propagation, the envelopes of the anisotropic random media have shorter duration and larger maximum amplitude than those of the isotropic random media. This implies that the intensity of the inhomogeneity is underestimated when one consider anisotropic lithosphere as isotropic random media.

ACKNOWLEDGMENTS

I thank H. Sato for leading my research interest in the study of seismogram envelopes and O. Nishizawa for his encouragement in the study of anisotropic media. Their comments are very helpful for improving this manuscript. I also thank M. Korn, U. Wegler and an anonymous reviewer for their helpful comments to the manuscript. This study was supported by JSPS and the Earthquake Research Institute cooperative research program.

REFERENCES

Aki, K. & Richards, P.G., 1980. *Quantitative Seismology*, W.H. Freeman, New York.

Chernov, L.A., 1960. *Wave Propagation in a Random Medium*, Mc-Graw Hill, New York.

Dolan, S.S., Bean, C.J. & Riollet, B., 1998. The broad-band fractal nature of heterogeneity in the upper crust from petrophysical logs, *Geophys. J. Int.*, **132**, 489–507.

Fehler, M., Sato, H. & Huang, L.-J., 2000. Envelope broadening of outgoing waves in 2-D random media: a comparison between the Markov approximation and numerical simulations, *Bull. seism. Soc. Am.*, **90**, 914–928.

Furumura, T. & Kennett, B.L.N., 2005. Subduction zone guided waves and the heterogeneity structure of the subducted plate: intensity anomalies in northern Japan, *J. geophys. Res.*, **110**, B10302, doi:10.1029/2004JB003486.

Hestholm, S.O., Husebye, E.S. & Ruud, B.O., 1994. Seismic wave propagation in complex crust-upper mantle media using 2-D finite-difference synthetics, *Geophys. J. Int.*, **118**, 643–670.

Holliger, K. & Levander, A., 1992. A stochastic view of lower crustal fabric based on evidence from the Ivrea zone, *Geophys. Res. Lett.*, **19**, 1153–1156.

Ikelle, L.T., Yung, S.K. & Daube, F., 1993. 2-D random media with ellipsoidal autocorrelation functions, *Geophysics*, **58**, 1359–1372.

Ishimaru, A., 1978. *Wave Propagation and Scattering in Random Media*, Academic Press, New York.

Iooss, B., 1998. Seismic reflection traveltimes in two-dimensional statistically anisotropic random media, *Geophys. J. Int.*, **135**, 999–1010.

Jannaud, L.R., Adler, P.M. & Jacquin, C.G., 1992. Wave propagation in random anisotropic media, *J. geophys. Res.*, **97**, 15 277–15 289.

Kamei, R., Hato, M. & Matsuoka, T., 2005. Random heterogeneous model with bimodal velocity distribution for methane hydrate exploration, *Butsuri-Tansa*, **58**, 41–49.

Kawahara, J., 2002. Cutoff scattering angles for random acoustic media, *J. geophys. Res.*, **107**(B1), 20120, doi:10.1029/2001JB000429.

Korn, M. & Sato, H., 2005. Synthesis of plane vector wave envelopes in two-dimensional random elastic media based on the Markov approximation and comparison with finite-difference simulations, *Geophys. J. Int.*, **161**, 839–848.

Kravtsov, Y.A., Müller, T.M., Shapiro, S.A. & Buske, S., 2003. Statistical properties of reflection traveltimes in 3-D randomly inhomogeneous and anisomeric media, *Geophys. J. Int.*, **154**, 841–851.

Lee, L.C. & Jokipii, J.R., 1975a. Strong scintillations in astrophysics: I. The Markov approximation, its validity and application to angular broadening, *Astrophys. J.*, **196**, 695–707.

Lee, L.C. & Jokipii, J.R., 1975b. Strong scintillations in astrophysics: II. A theory of temporal broadening of pulses, *Astrophys. J.*, **201**, 532–543.

Matsumoto, S., Obara, K. & Hasegawa, A., 2001, Characteristic of coda envelope for slant-stacked seismogram, *Geophys. Res. Lett.*, **28**, 1111–1114.

Müller, T.M. & Shapiro, S.A., 2003. Amplitude fluctuations due to diffraction and refraction in anisotropic random media: implications for seismic scattering attenuation estimates, *Geophys. J. Int.*, **155**, 139–148.

Obara, K. & Sato, H., 1995. Regional differences of random inhomogeneities around the volcanic front in the Kanto-Tokai area, Japan, revealed from the broadening of S wave seismogram envelopes, *J. geophys. Res.*, **100**, 2103–2121.

Ryberg, T., Tittgemeyer, M. & Wenzel, F., 2000. Finite difference modelling of *P*-wave scattering in the upper mantle, *Geophys. J. Int.*, **141**, 787–800.

Rytov, S.M., Kravtsov, Y.A. & Tatarskii, V.I., 1989. *Principles of Statistical Radio Physics (Vol. 4) Wave Propagation Through Random Media*, Springer-Verlag, Berlin.

Saito, T., Sato, H. & Ohtake, M., 2002. Envelope broadening of spherically outgoing waves in three-dimensional random media having power-law spectra, *J. geophys. Res.*, **107**(B5), 2089, doi:10.1029/2001JB000264.

Saito, T., Sato, H., Fehler, M. & Ohtake, M., 2003. Simulating the envelope of scalar waves in 2D random media having power-law spectra of velocity fluctuation, *Bull. seism. Soc. Am.*, **93**, 240–252.

Saito, T., Sato, H., Ohtake, M. & Obara, K., 2005. Unified explanation of envelope broadening and maximum-amplitude decay of high-frequency seismograms based on the envelope simulation using the Markov approximation: forearc side of the volcanic front in northeastern Honshu, Japan, *J. geophys. Res.*, **110**, B01304, doi:10.1029/2004JB003225.

Sato, H., 1982. Amplitude attenuation of impulsive waves in random media based on travel time corrected mean wave formalism, *J. acoust. Soc. Am.*, **71**, 559–564.

Sato, H., 1989. Broadening of seismogram envelopes in the randomly inhomogeneous lithosphere based on the parabolic approximation: Southeastern Honshu, Japan, *J. geophys. Res.*, **94**, 17 735–17 747.

Sato, H. & Fehler, M., 1998. *Seismic Wave Propagation and Scattering in the Heterogeneous Earth*, Springer-Verlag, New York.

Sato, H., Fehler, M. & Saito, T., 2004. Hybrid synthesis of scalar wave envelopes in two-dimensional random media having rich short-wavelength spectra, *J. geophys. Res.*, **109**, B06303, doi:10.1029/2003JB002673.

Scherbaum, F. & Sato, H., 1991. Inversion of full seismogram envelopes based on the parabolic approximation: Estimation of randomness and attenuation in southeastern Honshu, Japan, *J. geophys. Res.*, **96**, 2223–2232.

Shearer, P.M., 1999. *Introduction to Seismology*, Cambridge University Press, Cambridge.

Shiomi, K., Sato, H. & Ohtake, M., 1997. Broad-band power-law spectra of well-log data in Japan, *Geophys. J. Int.*, **130**, 57–64.

Tsukada, S., Odaka, T., Ashiya, K., Ohtake, K. & Nozaki, D., 2004. Analysis of the envelope waveform of the initial part of P-waves and its application to quickly estimating the epicentral distance and magnitude, *Zisin II*, **56**, 351–361 (in Japanese with English Abstract).

Wu, R.S., 1982. Attenuation of short period seismic waves due to scattering, *Geophys. Res. Lett.*, **9**, 9–12.

Wu, R.S., Xu, Z. & Li, X.-P., 1994. Heterogeneity spectrum and scale anisotropy in the upper crust revealed by the German continental deep-drilling (KTB) holes, *Geophys. Res. Lett.*, **21**, 911–914.

APPENDIX A: DERIVATION OF EQ. (16)

In this appendix, we derive the eq. (16) following the derivations of Lee & Jokipii (1975a) and Sato & Fehler (1998). From the parabolic eq. (12), we can write the wavefield at $(r_{\perp j}, r)$ by using the wavefield at $(r_{\perp j}, r - \Delta r)$,

$$\begin{aligned} U(r_{\perp j}, r, \omega_j) &\approx U(r_{\perp j}, r-\Delta r, \omega_j) + \frac{i}{2k_j}\int_{r-\Delta r}^{r} \frac{1}{r'^2}\frac{\partial^2}{\partial\phi^2} U(r_{\perp j}, r', \omega_j)dr' - ik_j\int_{r-\Delta r}^{r} \xi(r_{\perp j}, r')U(r_{\perp j}, r', \omega_j)dr' \\ &\approx U_j(r-\Delta r) + \frac{i}{2k_j}\frac{1}{r^2}\frac{\partial^2}{\partial\phi^2}U_j(r-\Delta r)\Delta r - ik_jU_j(r-\Delta r)\int_{r-\Delta r}^{r}\xi_j(r')dr', \end{aligned} \tag{A1}$$

where $U_j(r-\Delta r)$ and $\xi_j(r')$ mean $U(r_{\perp j}, r-\Delta r)$ and $\xi(r_{\perp j}, r')$, respectively. In the approximation used in eq. (A1), we suppose the existence of an intermediate scale Δr, which is larger than the scale of inhomogeneity along the r-axis, or the correlation distance, but smaller than the scale of variation of U along the r-axis. It should be noted that the second and third terms in the last equation are small compared to the first term. Neglecting smaller terms, we calculate an ensemble-averaged value as follows,

$$\begin{aligned} \langle\xi_1(r)U_1(r)U_2^*(r)\rangle &\approx \langle ik_2\xi_1(r)U_1(r-\Delta r)U_2^*(r-\Delta r)\int_{r-\Delta r}^{r}\xi_2(r'')\,dr''\rangle - \langle ik_1\xi_1(r)U_1(r-\Delta r)U_2^*(r-\Delta r)\int_{r-\Delta r}^{r}\xi_1(r')dr'\rangle \\ &\quad - \left\langle\frac{i\xi_1(r)\Delta r}{2k_2r^2}U_1(r-\Delta r)\frac{\partial^2}{\partial{\phi_2}^2}U_2^*(r-\Delta r)\right\rangle + \left\langle\frac{i\xi_1(r)\Delta r}{2k_1r^2}U_2^*(r-\Delta r)\frac{\partial^2}{\partial{\phi_1}^2}U_1(r-\Delta r)\right\rangle \\ &\quad + \langle\xi_1(r)U_1(r-\Delta r)U_2(r-\Delta r)\rangle \\ &\approx ik_2\langle U_1(r-\Delta r)U_2^*(r-\Delta r)\rangle\left\langle\int_{r-\Delta r}^{r}\xi_1(r)\xi_2(r'')dr''\right\rangle - ik_1\langle U_1(r-\Delta r)U_2^*(r-\Delta r)\rangle\left\langle\int_{r-\Delta r}^{r}\xi_1(r)\xi_1(r')\,dr'\right\rangle \\ &= ik_2\langle U_1(r-\Delta r)U_2^*(r-\Delta r)\rangle\int_0^{\Delta r}R(r_{\perp1}-r_{\perp2}, r')\,dr' - ik_1\langle U_1(r-\Delta r)U_2^*(r-\Delta r)\rangle\int_0^{\Delta r}R(0, r')dr' \\ &\approx \frac{1}{2}ik_2\langle U_1(r-\Delta r)U_2^*(r-\Delta r)\rangle\int_{-\infty}^{\infty}R(r_{\perp1}-r_{\perp2}, r')dr' - \frac{1}{2}ik_1\langle U_1(r-\Delta r)U_2^*(r-\Delta r)\rangle\int_{-\infty}^{\infty}R(0, r')dr' \\ &\approx \frac{i}{2}\left\{k_2A(r_{\perp1}-r_{\perp2}, \phi) - k_1A(0, \phi)\right\}\Gamma_2. \end{aligned} \tag{A2}$$

At the derivation of the third equation, the causality deduced from the forward scattering approximation is used; there is no contribution of the inhomogeneity at r to the wavefield at $r-\Delta r$. At the derivation of the fifth equation, the integration at the fourth equation is approximated by the infinite integration since we supposed Δr is larger than the correlation distance. Also, we supposed $R(r_{\perp k}-r_{\perp m}, -r'') \approx R(r_{\perp k}-r_{\perp m}, r'')$ in weakly anisotropic random media considering that the contribution of $R(r_{\perp k}-r_{\perp m}, r'')$ is larger as $|r_{\perp k}-r_{\perp m}|$ become smaller. At the derivation of the last equation, we suppose $\langle U_1(r-\Delta r)\,U_2^*(r-\Delta r)\rangle \approx \langle U_1(r)\,U_2^*(r)\rangle$ considering the existence of small Δr which is smaller than the scale of variation of U along the r-axis. By using the eq. (A2), we obtain the following relation,

$$\left\langle(k_1\xi_1 - k_2\xi_2)U_1U_2^*\right\rangle \approx -\frac{i}{2}\left[\left({k_1}^2+{k_2}^2\right)A(0, \phi) - 2k_1k_2A(r_{\perp1}-r_{\perp2}, \phi)\right]\Gamma_2. \tag{A3}$$